Applied Catalysis B: Environmental 150–151 (2014) 370–379

Contents lists available at ScienceDirect

Applied Catalysis B: Environmental

journal homepage: www.elsevier.com/locate/apcatb

Stainless steel wire mesh-supported Co_3O_4 catalysts in the steam reforming of ethanol

Laura del Río, Irene López, Gregorio Marbán*

Instituto Nacional del Carbón (INCAR-CSIC), c/Francisco Pintado Fe 26, 33011 Oviedo, Spain

ARTICLE INFO

Article history:
Received 18 October 2013
Received in revised form 5 December 2013
Accepted 13 December 2013
Available online 21 December 2013

Keywords:
Ethanol steam reforming
Hydrogen
Cobalt
Potassium
Micro-reactor

ABSTRACT

Structured catalysts consisting of either undoped or potassium-doped mesoporous Co_3O_4 nanowires supported on stainless steel wire meshes (SSWM) and prepared by the ammonia evaporation-induced method were tested in the ethanol steam reforming (ESR) reaction. The undoped catalyst was strongly reduced to elemental Co in ESR conditions, causing a decrease in catalytic activity, the undesired formation of acetone, the premature deactivation of the catalyst due to coke deposition and the detachment of particles from the SSWM. Doping the catalyst with potassium (molar K/Co around 0.05) produced an increase in the surface area of the catalysts and a significant enhancement of the catalytic performance in terms of H_2 TOF, carbon selectivity towards CO_2 and stability. The presence of potassium prevented the over-reduction of the Co_3O_4 particles to elemental Co, thereby avoiding the detrimental effects of this phase. Comparison with cobalt-based catalysts described in the literature confirm that the doped catalysts produced in this work are more active and present better values of carbon selectivity towards CO_2 than structured catalysts previously reported.

1. Introduction

In situ hydrogen production from bio-ethanol in fuel cell-based vehicles is an attractive option towards a carbon-free transport future [1]. It can be carried out inside the vehicle with catalytic systems by means of steam reforming, partial oxidation or auto-thermal reforming [2,3]. A large number of works on the production of hydrogen from ethanol involve the steam reforming process with catalysts based on noble metals, such as rhodium, platinum, iridium, palladium and ruthenium as well as non-noble metals, such as cobalt, nickel and copper [4–6]. Cobalt-based catalysts have been extensively studied over the last fifteen years for the steam reforming of ethanol (SRE), since they show the highest activity and selectivity towards hydrogen. In fact, cobalt-based catalysts show a similar activity to noble metals in C–C bond cleavage, even at temperatures as low as 400 °C [7]. Catalysts based on noble metals are ideal for avoiding coke formation, though they are costly and need high temperatures to be active (650–750 °C) [8]. On the other hand cobalt-based catalysts are cheap and active at low temperatures (250–550 °C), but deactivate quickly due to coke generation. In this context, the search for cobalt-based catalysts for ESR that do not generate coke and therefore do not deactivate continues to be an open issue.

Doping the cobalt oxides with potassium has been presented as a promising way to improve catalytic selectivity towards H_2 and CO_2 and to reduce coke deposition at low temperatures [9–11]. According to Pereira et al. [11] cobalt reduction to small Co^0 particles is favoured by using potassium as a promoter. In other studies it has been shown that cobalt(II) oxide is essentially inactive in ESR, and low temperature steam reforming activity was observed when the oxide was reduced to elemental cobalt [12–14]. In contrast, recent studies [9,10] have revealed that CoO plays an important role in the ESR reaction. With the catalytic system used in these works (cobalt-exchanged hydrotalcites), the minute formation of elemental cobalt during the ESR process is thought to be responsible for the undesired deposition of coke. Thus it seems that the role of the cobalt oxidation state is a source of controversy in the ESR literature. One of the objectives of the present study is to shed light on this specific aspect of the use of cobalt-based catalysts in the ESR reaction.

Most of the works on cobalt-based catalysts for ESR are focussed on particulate catalysts. However, to put these catalysts into practice it is essential to build structured catalytic systems which are easy to handle, cause practically no pressure drop and show enhanced properties of mass and heat transport. Only a few works have dealt with the use of cobalt oxide catalysts dispersed on structured supports: cordierite monoliths [8–10,15–17], stainless

* Corresponding author. Tel.: +34 985119090; fax: +34 985297662.
E-mail address: greca@incar.csic.es (G. Marbán).

0926-3373/$ – see front matter © 2013 Elsevier B.V. All rights reserved.
http://dx.doi.org/10.1016/j.apcatb.2013.12.022

steel micro-reactors [17], silicon micro-monoliths [17,18] and membrane reactors [19]. Poor heat transfer efficiency, complex catalyst coating methods, frequent occurrence of hot spots and comparatively low catalytic efficiency are the main obstacles to the development of micro-reactor technology. Stainless steel wire-mesh (SSWM)-supported metal oxide catalysts have been revealed in the recent years as a very promising structured catalytic system [20–25]. The mesh in this type of catalyst provides a higher geometric surface area for supporting the active phase and allows a larger amount of catalyst per volume to be supported than the standard micro-channel reactors. SSWM-supported catalysts are also flexible enough to be fit into any kind of reactor, while ensuring a low pressure drop and good heat transfer. The primary aim of the present study was to test the use of SSWM-supported mesoporous cobalt oxide catalysts for the steam reforming of ethanol to produce hydrogen. To this end we analyzed the effect of doping the catalysts with potassium on their activity, selectivity and stability, and compared their performance with that of cobalt-based catalysts described in the literature.

2. Experimental

2.1. Catalyst synthesis

SSWM-supported Co_3O_4 catalysts were synthesized by the ammonia evaporation induced method at 90 °C for 18 h using $Co(NO_3)_2{\cdot}6H_2O$ (98%, Sigma Aldrich) as cobalt precursor and stainless steel wire mesh [with a wire diameter of 30 μm and a screen opening of 40 μm] provided by CISA as structured support. A detailed description of the synthesis procedure can be found elsewhere [21,22].

Before calcination, the cobalt was in the form of cobalt hydroxide on the surface of the SSWM. The uncalcined material was impregnated with potassium by the dropwise addition of an aqueous solution of K_2CO_3 (0.21 M). After the sample had been wetted, any excess solution was removed by air-blowing, followed by vacuum-drying at 60 °C for 1 h. The impregnation step was then repeated in order to obtain the desired amount of potassium in the catalyst. The molar ratio of potassium to cobalt (K/Co) ranged between 0 and 0.09. Finally all the samples were calcined in air at 350–400 °C for 2 h. The average amount of cobalt oxide in the SSWM-supported catalysts was 46 ± 4 wt%.

2.2. Catalyst characterization

The metal contents of the samples were determined by atomic absorption spectroscopy (AAS) and mass spectrometry (ICP–MS). Microscopic images of the samples were obtained using a scanning electron microscope (Zeiss, DSM 942 model). X-ray diffraction (XRD) analyses were carried out on a Bruker instrument (D8 Advance) operating at 40 kV and 40 mA and using Cu *K*α radiation (λ = 0.15406 nm). Crystal size values (d_{XRD}) were estimated from the XRD patterns by means of Scherrer's equation. N_2 adsorption isotherms at 77 K were obtained using a Micromeritics ASAP 2010 volumetric adsorption system. The BET surface area was determined from the isotherm analysis in the relative pressure range of 0.04 to 0.20. Ex-situ X-ray photoelectron spectroscopy (XPS) was carried out on a Specs spectrometer, with Mg-*K*α or Al-*K*α (30 eV) radiation emitted from a double anode at 50 W. The binding energies of the resulting spectra were corrected with the binding energy of adventitious carbon (284.6 eV) in the C 1s region. The backgrounds were subtracted by means of Shirley baselines. All the analyzed regions were deconvolved by mixed Gaussian–Lorentzian functions (90:10). To carry out quantitative analyses the atomic sensitivity factors stored in the CasaXPS database (v2.3.12Dev6) were used.

2.3. Catalytic deactivation and activity tests

The deactivation tests were performed using a quartz reactor placed inside a vertical furnace. A scheme of the reaction system is shown in Fig. 1. The catalyst was rolled up and introduced into a stainless steel tube (1/4 in. outer diameter) which was then placed inside the quartz reactor. The reaction mixture was passed through the catalyst and the particles detached during reaction were collected in a crucible located on the bottom of the quartz reactor. The vapour mixture (2 vol% EtOH and 12 vol% H_2O) was introduced by bubbling a nitrogen flow through a flask containing a liquid mixture of ethanol and water. In order to ensure that the ratio of ethanol vapour to water vapour remained constant the experiments were performed at 400 °C for only 2 h at a weight hourly space velocity of 1.64 (in units of $g_{EtOH}\ g_{Co_3O_4}{}^{-1}\ h^{-1}$ or, simply, h^{-1}). All the samples that passed the deactivation test (meaning that no particle detachment was detected) were subjected to the catalytic activity tests.

Catalytic activity tests for ESR were performed in a six-flow parallel micro-reactor system that allows up to six samples to be tested simultaneously by means of an automatically operated multiposition valve. Each catalyst consisted of a 5 cm × 1 cm strip that was rolled up to form a 1 cm-long cylindrical piece. One roll of catalyst was then inserted into each of the six stainless-steel reactors (1/4 in. outer diameter). A stream composed of 1.83 vol% ethanol, 11 vol% H_2O, 0–1.4 vol% O_2 and 10 vol% Ar in helium was fed into each reactor at weight hourly space velocities varying in the range 0.7–0.9 h^{-1}, depending on the small differences in the amount of catalyst loaded onto the metal wire mesh and on the total gas flow passed through each micro-reactor. In two cases the spatial velocity was increased to ~2.8 h^{-1} in order to obtain higher turnover frequencies at ethanol conversions below 100% so as to facilitate the comparison of the catalysts (Section 3.4). The samples were first heated at the reaction temperature in a flow of He for 30 min. Then the reactant stream was passed through the catalysts and their catalytic activity and selectivity were evaluated at temperatures ranging from 200 to 400 °C, in at least 7-hourly isothermal steps, although it was generally found that 1 h after each change in conditions the conversion levels were constant and could thus be considered as steady-state values. The transition ramp between each temperature step was performed under a helium atmosphere. The composition of the exiting gas mixtures was analyzed online by mass spectrometry (OmniStar 3000). Ethanol, H_2O, O_2, CO_2, CO and CH_4 were quantitatively analyzed with the help of previous calibration steps, while the evolution of the other byproducts (C_2 and C_3 species) was followed from the changes in the mass intensities of the corresponding fragments (i.e. 43 and 58 for acetone). By means of this procedure it was possible to know for certain whether any products other than CO_2 had formed during the reaction. Mass balances also allowed the concentration of these byproducts to be evaluated. The conversion parameter (X_{EtOH}; %) represents the percentage of ethanol converted according to the reaction (R1) taking into account the difference between the total flow rates at the outlet and the inlet of the reactor (F^{out} and F^{in}, respectively):

$$C_2H_5OH + 3(1-a)H_2O + (3/2)a\,O_2 \rightarrow 2\,CO_2 + (6-3a)H_2 \quad \text{(R1)}$$

$$X_{EtOH} = 100 \times \left(1 - \frac{F^{out}}{F^{in}} \frac{C^{out}_{EtOH}}{C^{in}_{EtOH}}\right) \quad (1)$$

where $C_{EtOH}{}^{in}$ and $C_{EOH}{}^{out}$ are the concentrations of ethanol (vol%) in the inlet and in the outlet gas stream, respectively. F^{out}/F^{in} can be evaluated as follows:

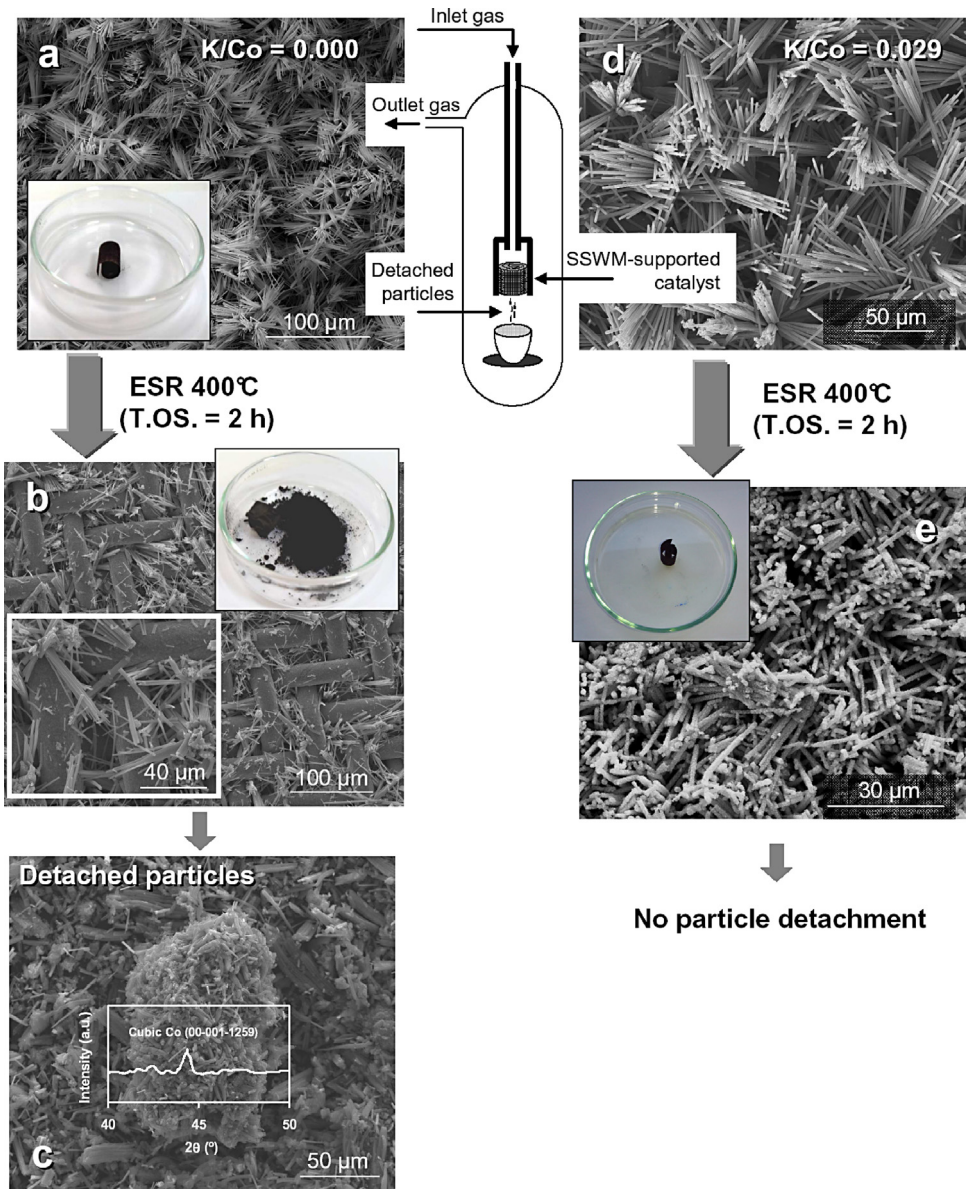

Fig. 1. Experimental setup for catalyst deactivation tests and photographs and SEM images of an undoped and a doped catalyst before and after the ESR reaction. The XRD spectrum of the particles detached from the undoped catalyst during the ESR is also provided.

$$\frac{F^{out}}{F^{in}} = \frac{100 - \sum_i (1 - 0.5\rho_i - 0.5\mu_i + 1.25\,\nu_i)\,C_i^{in}}{100 - \sum_i (1 - 0.5\rho_i - 0.5\mu_i + 1.25\,\nu_i)\,C_i^{out}} \quad (2)$$

where C_i^{in} and C_i^{out} are the concentrations of all the species i (vol%), except the inert gases, in the inlet and in the outlet gas stream, respectively, and ρ_i, μ_i and ν_i are the number of atoms of oxygen, hydrogen and carbon per molecule of species i. For reacting mixtures that are highly diluted in an inert gas (as in the case of this work) F^{out}/F^{in} parameter is always very close to unity. On the other hand, for non-diluted reacting mixtures the value of F^{out}/F^{in} can differ significantly from 1, considerably affecting the calculation of the ethanol conversion by Eq. (1). For instance, for a mixture of 14 vol% EtOH and 84 vol% H_2O reacting according to (R1) assuming 50% ethanol conversion, the value of F^{out}/F^{in} is 1.24. To the best of our knowledge, this is never taken into account in the literature on the steam reforming of ethanol. Each experimental conversion point was evaluated after more than 7 h of reaction at a specified temperature.

The activity of the catalysts towards H_2 formation was evaluated by the TOF × d parameter $\left(g_{H_2}\ g_{Co}^{-1}\ s^{-1}\right)$, where TOF is the *turnover frequency* and d is the dispersion of the active phase. TOF × d was calculated from the following equation:

$$\text{TOF} \times d = \frac{2F_{H_2}^{out}}{w_{Co}} \quad (3)$$

where $F_{H_2}{}^{out}$ is the outlet H_2 molar flow (mol s^{-1}) and w_{Co} is the mass of cobalt in the catalyst (g_{Co}). The parameter TOF × d is more efficacious than the standard TOF when comparing the catalytic activity of different catalysts since it considers the rate of H_2 production per *total* mass of cobalt and not only per *exposed* mass of cobalt. Furthermore dispersion (d) is a property not usually evaluated or reported in the literature, and therefore the standard TOF cannot usually be evaluated on the basis of the available

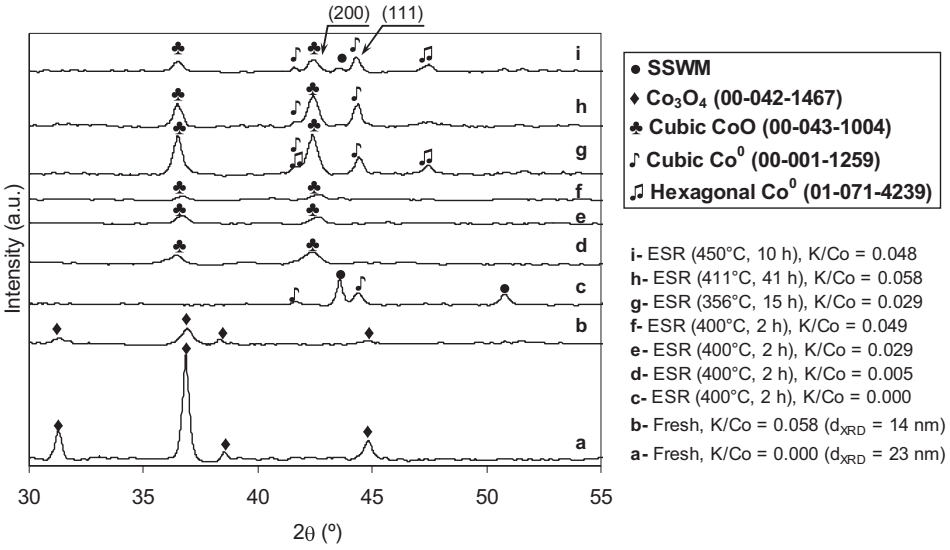

Fig. 2. XRD spectra for different catalyst samples before and after the ESR reaction under different conditions.

data. According to reaction (R1), the maximum achievable value of TOF × d is:

$$\mathrm{TOF} \times d\big|_{\max} = \frac{2\,(6-2a)\,F_{\mathrm{EtOH}}^{\mathrm{in}}}{w_{\mathrm{Co}}} \tag{4}$$

Therefore, the hydrogen yield (%) can be evaluated as:

$$X_{\mathrm{H_2}} = 100 \times \frac{\mathrm{TOF} \times d}{\mathrm{TOF} \times d\big|_{\max}} = 100 \times \frac{F_{\mathrm{H_2}}^{\mathrm{out}}}{F_{\mathrm{EtOH}}^{\mathrm{in}}(6-2a)} \tag{5}$$

where $F_{\mathrm{EtOH}}{}^{\mathrm{in}}$ is the inlet ethanol molar flow (mol s^{-1}).

Finally, we define the carbon selectivity (S^{C}_{Pi}; %) towards each possible carbon-containing product Pi as the molar percentage of each carbon-containing product evolved (CO_2, CO, CH_4, etc.) with respect to the total amount of moles of the carbon-containing products formed.

$$S_{\mathrm{Pi}}^{\mathrm{C}} = 100 \times \frac{\nu_{\mathrm{Pi}} C_{\mathrm{Pi}}}{\sum_{\mathrm{Pi}} \nu_{\mathrm{Pi}} C_{\mathrm{Pi}}} \tag{6}$$

where ν_{Pi} is the number of carbon atoms in the carbon-containing molecule Pi of the reaction products.

3. Results and discussion

3.1. Structural characterization of the fresh catalyst samples

The SSWM-supported Co_3O_4 catalysts show typical flower-like mesoporous nanowire arrays (mean pore diameter ~3.4 nm) that are evenly spaced over the metal wire meshes [20,22] (Fig. 1a and d). The XRD spectra of both the undoped and the K-doped samples (Fig. 2a and b) show the Co_3O_4 spinel structure. Doping with potassium provokes a decrease in the crystal size of Co_3O_4 (Fig. 2 legend) and a corresponding increase in the specific surface area from around 30 $m^2\,g^{-1}$ to around 50 $m^2\,g^{-1}$ (molar K/Co > 0.02), on a cobalt oxide mass basis. This result is similar to those obtained by other authors [26]. XPS analyses can help to determine the distribution of potassium on the SSWM-supported Co_3O_4 samples. Fig. 3a shows the variation of the C/Co atom ratio with the K/Co atom ratio on the surface of the K-doped samples obtained using two X-ray sources of different penetration power (Mg-$K\alpha$ and Al-$K\alpha$). The Al source produces X-rays with a higher penetration power than the Mg source and therefore provides slightly more information on the "bulk" of the particles than the latter. The samples used for these analyses have a theoretical molar K/Co ratio in the range 0.01–0.06. The K/Co values obtained by XPS are consistently higher than 0.07 (Fig. 3a) which agrees with the fact that the potassium is placed on the external surface of the catalyst and not incorporated into the bulk. This is corroborated by the different trends obtained by both X-ray sources. The higher values of K/Co obtained by the Al source (Fig. 3a) is firm evidence that potassium is concentrated on the external surface of the spinel. There is also a large amount of carbon on the surface of the fresh Co_3O_4 nanorods. This might

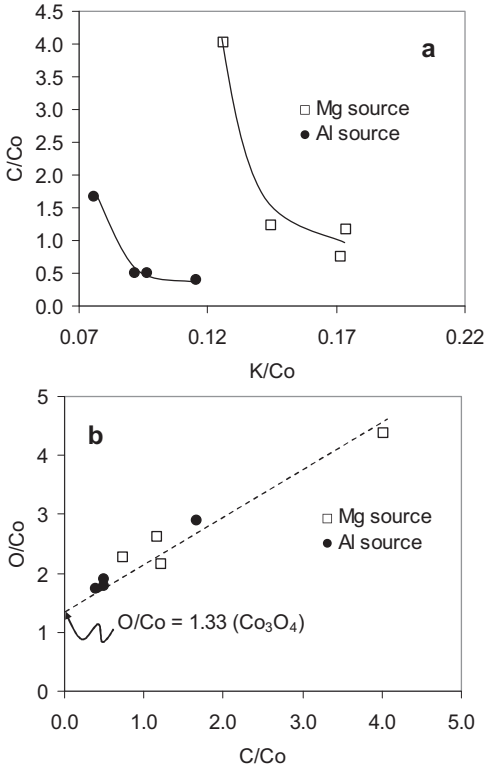

Fig. 3. Surface composition of the doped catalysts evaluated by XPS with two different radiation sources. a) C/Co *vs.* K/Co and b) O/Co *vs.* C/Co.

Table 1
Deactivation tests.

Molar K/Co	0.000	0.005	0.029	0.049
XRD phases on the mesh	Cubic Co, SSWM	Cubic CoO	Cubic CoO	Cubic CoO
Detached particles (wt%)	74.1	11.2	0	0
XRD phases in the detached particles	Cubic Co	Cubic Co	–	–
%C in the detached particles	40.5	12.5	–	–

Catalyst properties after the ESR reaction (400 °C, T.O.S. = 2 h) for catalysts doped with different amounts of potassium.

suggest that the potassium carbonate was not properly decomposed during the calcination stage. Surprisingly the catalyst which shows the highest C/Co ratio in Fig. 3a is the one with the lowest potassium content and the one that was calcined at the highest temperature (400 °C *vs.* 350 °C for the other catalysts). Consequently the carbon content must be a result of the adsorption of atmospheric CO_2 in the form of carbonates or other carbon-containing species over the cobalt atoms. As can be seen in the figure, the surface potassium provokes a significant decrease in the amount of adsorbed carbon. This might be an early indication of the role of potassium during the steam reforming of ethanol.

Fig. 3b shows the variation of the O/Co atom ratio with the C/Co atom ratio on the surface of the K-doped samples. The clear trend revealed by both X-ray sources indicates that the high amount of oxygen on the surface of the catalyst must be due mainly to the presence of carbon, which confirms the origin of this contamination. Thus, when extrapolating the trend to C/Co = 0, the expected value of O/Co = 1.33, corresponding to the Co_3O_4 spinel is obtained.

3.2. *Effect of potassium on the deactivation of SSWM-supported Co_3O_4 catalysts*

The results of the deactivation tests performed in the quartz reactor (see Section 2) are essential to understand the role of potassium in the reaction mechanism. Fig. 1 shows SEM images of two samples, one undoped (Fig. 1a) and another with a molar K/Co ratio of 0.029 (Fig. 1d). Both samples have a similar morphology before the reaction from a macroscopic point of view. After only 2 h of ESR reaction at 400 °C the undoped catalyst suffered the detachment of a massive amount of particles from the wire mesh (Fig. 1b), amounting to about 74 wt% of the Co_3O_4 initially stuck to the mesh (Table 1). The XRD spectrum of this spent mesh (Fig. 2c) is formed by the peaks of the stainless steel wire mesh that, as it is now partially uncovered, is accessible to the X-rays, and the peaks of the cubic elemental cobalt, there being no other discernible cobalt phases being. This evidences that the Co_3O_4 particles in the undoped catalyst were massively reduced to elemental cobalt during the ESR reaction, and that most of them have been dislodged from the wire mesh. As indicated in Table 1, the detached particles, an image of which can be seen in Fig. 1c, are formed by elemental cobalt and a large amount of carbon (around 40 wt%). It seems that elemental cobalt is detrimental to the ESR reaction in two ways, firstly in that it promotes the detachment of particles from the wire mesh and secondly in that it favours the deposition of coke on the surface of the particles. Doping of the catalyst with potassium prevents both of these phenomena, as can be deduced from the data in Table 1. The presence of potassium prevents the Co_3O_4 particles from being reduced to elemental cobalt in the ESR conditions employed in the deactivation tests. TPR analyses performed in a previous work [22] proved that the temperature necessary to reduce Co^{2+} to Co^0 is higher when potassium in present. For this reason, the only phase detected by XRD in the doped catalysts subjected to the ESR reaction in the deactivation tests (T.O.S. = 2 h) is cubic CoO (Fig. 2d–f and Table 1). For the lowest degree of K doping (K/Co = 0.005) there is still some detachment of particles from the wire mesh (~11 wt%; Table 1), which has ceased for higher K/Co ratios (Table 1). It should be noted that the XRD phase of these detached particles is Co^0 but the amount of coke deposited on their surface is much lower than the amount deposited on the surface of the Co^0 particles detached from the undoped catalyst (12.5 *vs.* 40.5 wt%; Table 1). Potassium therefore not only minimizes the over-reduction of Co_3O_4 to elemental cobalt, but also limits the formation of coke deposits on the surface of the Co^0 particles.

The catalyst samples subjected to ESR for longer reaction times in the six-flow parallel micro-reactor system were also characterized. After 15 h of reaction at 350 °C XRD analysis of the doped sample revealed the presence of some elemental cobalt, in the form of a mixture of hexagonal and cubic Co^0 in conjunction with the predominant CoO phase (Fig. 2g). At a higher reaction temperature (400 °C) the hexagonal Co^0 was almost completely transformed to cubic Co^0 (Fig. 2h). This suggests that a small amount of the CoO is slowly reduced to Co^0 during the ESR reaction, so that it cannot be detected after just 2 h reaction (Fig. 2d–f) whereas it is clearly visible after longer reaction times (Fig. 2g and h). In the view of this it is surprising that the elemental cobalt is not detected in the XPS analyses of the doped samples subjected to long term ESR reaction. Fig. 4 shows the Co 2p region of the XPS spectra for a doped catalyst (K/Co = 0.048) before (fresh sample) and after ESR reaction (350 °C, 15 h), obtained using the Mg-*K*α source. The energy gaps between the Co 2p main peaks and the satellite peaks are related to the oxidation states. When the energy gap is ~6.0 eV, the Co cation valence is assigned a value of 2+, whereas if the energy gap is 9–10 eV, the spectrum is associated with Co cations that have a valence of 3+ [27]. As can be observed in Fig. 4 each satellite peak for the fresh sample in the Co $2p_{3/2}$ and Co $2p_{1/2}$ regions is the summation of two different peaks. Calculation of the energy gaps taking into account these peaks results in a mixture of two energy gaps (5.4–6.6 and 8.8–10.0) which corresponds fairly well to the composition of the Co_3O_4 spinel (Fig. 4). On the other hand, the XPS spectrum of the sample subjected to ESR at 350 °C for 15 h, only shows one energy gap with a value of around 6 (5.6–6.2), as might be expected for CoO. As mentioned before, the peak for elemental cobalt, which is known to be situated at 777.8–778.4 eV [28–30] in the Co $2p_{3/2}$ region is absent in the spectra shown in Fig. 4.

In order to reconcile the XPS results with the XRD data only two possible explanations can be contemplated; (i) Co^0 is present inside the bulk of the catalyst particles but not on their external surface and/or (ii) Co^0 on the external surface is covered by coke which masks its presence in the XPS analysis. The first hypothesis implies that the elemental cobalt located on the external surface is oxidized during the room temperature handling of the catalyst between the ESR reaction and the XPS analysis. However, the Al-*K*α source in the XPS equipment, despite having a greater power of penetration, is still unable to detect any trace of elemental cobalt in the reacted sample (Fig. S1 in supplementary information). The assumption that coke deposits are masking the surface Co^0 is supported by the increase in the C/Co molar ratio as a consequence of the reaction (from 1.2 to 4.4, as indicated in Fig. 4). This suggests

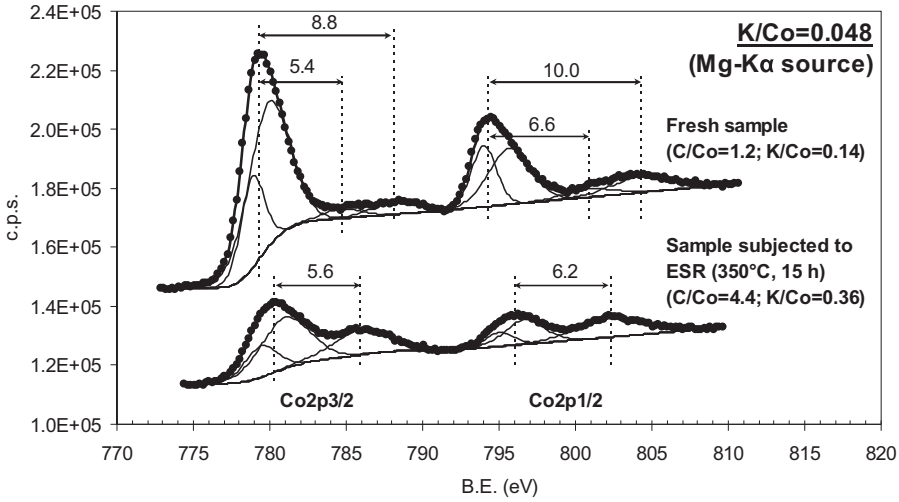

Fig. 4. Co 2p spectra for a doped catalyst (K/Co = 0.048) before and after the ESR reaction.

that the formation of coke deposits mainly occurs on the surface of the elemental Co particles. The small and undesired presence of Co^0 after a long term ESR reaction might be ascribed to an uneven distribution of potassium on the surface of the catalyst as a consequence of the impregnation method used (dropwise impregnation). Thus, the areas of the spinel which are well impregnated with potassium do not experience over-reduction to Co^0, whereas those on which potassium has not been appropriately distributed are reduced during the ESR reaction. This uneven distribution is also implied by the value of the atomic K/Co ratio obtained from the XPS results (Fig. 4). For the fresh sample this value is 0.14 (always higher than the input value, as mentioned before), whereas after being subjected to the ESR reaction it increased to 0.36, which means that the exposed CoO is richer in potassium than the covered Co^0. It might be worthwhile using other potassium impregnation methods, such as equilibrium impregnation, which, while adding complexity to the procedure, would improve the distribution of potassium on the catalyst surface and therefore minimize the undesired formation of elemental cobalt. In summary, the presence of potassium on the catalyst surface prevents its over-reduction to elemental cobalt, the phase which is responsible for both the detachment of particles from the wire mesh and the deactivation of the catalyst through coke deposition.

3.3. Catalytic performance of potassium-doped SSWM-supported Co_3O_4 catalysts

Fig. 5 shows the variation of the hydrogen yield and the carbon selectivity towards CO_2 with temperature, evaluated from Eqs. (5) and (6), for different SSWM-supported Co_3O_4 catalysts tested at spatial velocities of around 0.8 h^{-1}. As can be observed, the undoped catalyst has a much lower hydrogen yield than the potassium-doped catalysts. The latter show hydrogen yields close to 90% at temperatures in the 330–350 °C range. It was not possible to evaluate the activity of the undoped catalyst at other temperatures because the detachment of particles caused the micro-reactor to malfunction. The carbon selectivity of this catalyst towards CO_2 was also much lower than that of the doped catalysts (inset in Fig. 5), in accordance with the results obtained by Espinal et al. [9–11], with relatively high values of carbon selectivity towards CO (~10–11%), CH_4 (12–14%) and acetone (~15%) in the range of temperatures analyzed. The doped catalysts presented values of carbon selectivity towards CO_2 of over 90% at temperatures slightly over 300 °C. This suggests that the CoO phase, which is predominant in the doped catalysts during the ESR reaction, is more active and selective towards CO_2 than the Co^0 phase of the undoped catalysts.

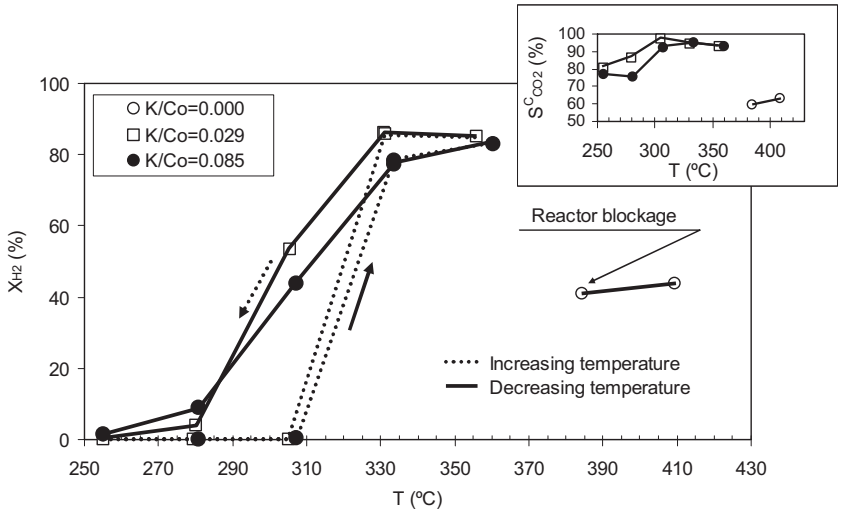

Fig. 5. Hydrogen yield and carbon selectivity towards CO_2 (inset) *vs.* temperature for the doped and undoped catalysts.

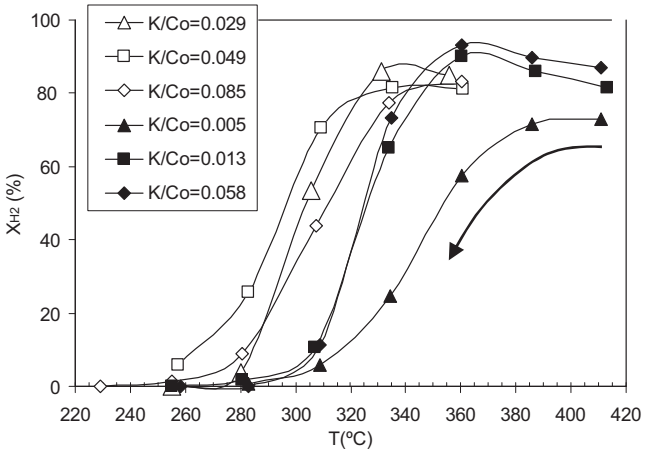

Fig. 6. Variation of hydrogen yield with temperature for the doped catalysts tested at decreasing temperatures from 350 to 400 °C.

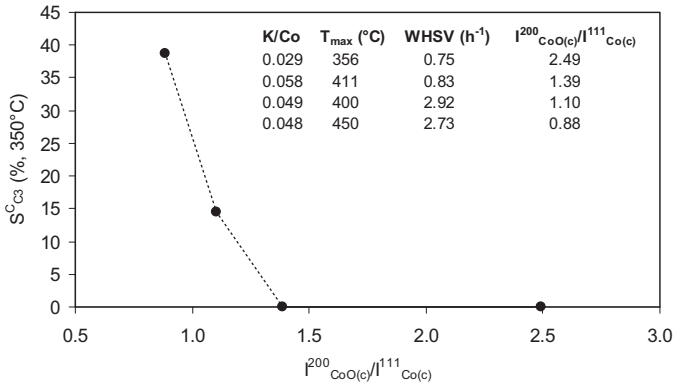

Fig. 7. Variation of carbon selectivity towards acetone at 350 °C with the relative amounts of CoO to Co in the doped catalysts.

The catalysts tested in this work were not subjected to a pre-reduction treatment. Thus, the hysteresis loops observed in Fig. 5 for the doped catalysts were a consequence of the onset of reduction of Co_3O_4 to CoO, that occurred in all cases in the 300–310 °C range (Fig. 5).

Fig. 6 shows the hydrogen yield curves at decreasing temperatures for some of the catalysts doped with different amounts of potassium (WHSV~0.8 h 1) included in Table 2. Those catalysts that have not been subjected to temperatures above ~350 °C are more active in the 260–340 °C temperature range than those tested at temperatures up to 400 °C, probably due to a higher degree of sintering of the active phase at the highest temperature.

Table 2 shows the values of ethanol conversion, carbon selectivity and hydrogen yield at different temperatures corresponding to the doped catalysts tested in this work. In general the values of selectivity towards CO_2 were excellent for all the doped catalysts tested at ~400 °C or lower maximum temperatures, with only the minute formation of CO and acetone, and only at the lowest reaction temperatures (Table 2). Only for the two catalysts tested at the highest space velocity (~2.8 h^{-1}), was considerable selectivity towards the formation of acetone detected. Certainly one of these catalysts was subjected to a maximum ESR temperature of 450 °C, which may have altered its surface composition, but the other catalyst did not undergo temperatures over 400 °C and still a noticeable amount of acetone was detected. To explain this, XRD analyses of both treated catalysts were performed. Fig. 2i shows the XRD spectrum of the catalyst subjected to a maximum temperature of 450 °C. As can be observed, the intensity ratio of peak (2 0 0) for cubic CoO to peak (1 1 1) for cubic elemental Co ($I^{200}{}_{CoO(c)}/I^{111}{}_{Co(c)}$) appears to be lower in these treated catalysts than in the catalysts subjected to lower maximum temperatures. It seems that the presence of elemental cobalt not only affects the detachment of particles and coke deposition, but also provokes the undesired formation of acetone. To confirm this, Fig. 7 plots the variation of carbon selectivity towards acetone at 350 °C *vs.* the $I^{200}{}_{CoO(c)}/I^{111}{}_{Co(c)}$ parameter for the catalysts whose characteristics are shown in the same figure. As can be observed for the $I^{200}{}_{CoO(c)}/I^{111}{}_{Co(c)}$ values over ~1.4 carbon selectivity towards acetone is zero. The relative amount of CoO to Co^0 is not only affected by temperature but also by the space velocity. Thus, as can be seen in Fig. 7, the catalyst tested at a maximum temperature of 400 °C and WHSV = 2.92 h^{-1} presents a lower value of $I^{200}{}_{CoO(c)}/I^{111}{}_{Co(c)}$ (a higher relative amount of Co^0) than a similar catalyst tested at a similar maximum temperature (411 °C) but at a lower WHSV (0.83 h^{-1}). This is a consequence of the higher amount of hydrogen in the environment of the catalyst tested at the higher space velocity, as revealed by the TOF × *d* values at ~400 °C at low $\left(\sim 7 \times 10^{-5}\ g_{H_2}\ g_{Co}{}^{-1}\ s^{-1}\right)$ and high $\left(1.5 \times 10^{-4}\ g_{H_2}\ g_{Co}{}^{-1}\ s^{-1}\right)$ space velocities (Table 2). It can be inferred from this that the conditions for selectively employing these catalysts must be chosen so that the final $I^{200}{}_{CoO(c)}/I^{111}{}_{Co(c)}$ value is higher than, or equal to, 1.4.

The stability of the catalysts was also remarkable. As can be seen in Table 2, when returning to the same reaction temperature after many hours the hydrogen yields were equal to, or higher than, in the previous reaction step.

3.4. Comparison with other cobalt-based catalysts

It is a known fact that the term "conversion" is wrongly used as a synonym for "activity" in many catalysis works, in which a good catalyst is one that produces a high "conversion" of reagents in products at a low temperature. However catalytic activity, expressed either as a kinetic rate constant or as a turnover frequency, depends not only on conversion but also on spatial velocity and reagent concentration. It is very rare to find in the literature works that compare the catalytic activity of the analyzed catalysts with that of those previously described in the literature. It is our practice to attempt such comparisons [20–22,31,32], and shall do so in the present section, which will serve as a short review of cobalt-based catalysts analyzed for the ethanol steam reforming reaction. From the extensive literature on the subject, around 70 works, only in 38 was it possible to use the data reported to derive the values of TOF × *d* as explained in Section 2. The best catalysts described in these works are listed in Table S1 (Supplementary information), together with the testing conditions and the results for ethanol conversion (X_{EtOH}), carbon selectivity $\left(S^C_{Pi}\right)$, hydrogen yield $\left(X_{H_2}\right)$ and TOF × *d* on a Co mass basis. To rank these catalysts according to their performance on the basis of these data is a complicated task since the conditions used involved complete ethanol conversion in many cases (Table 2). Therefore, to ensure a sound comparison, only the data for 10% to 85% ethanol conversion were used.

Fig. 8 shows the values of TOF × *d* (on a Co mass basis) for the catalysts indicated in Table S1. It can be seen that the top performing catalysts (highlighted in Table S1) follow a clear trend that can be expressed by the equation indicated in the figure. These catalysts, which are all in particulate form, are also the top ones when their values of TOF × *d* are expressed on a total catalyst mass basis (Fig. 9), with the exception of that reported in the work by Moura et al. [7], whose TOF × *d* value decreased considerably and was therefore not used for plotting the linear trend in Fig. 9. Furthermore, cobalt in this catalyst is located in the support, and not on the external surface [7]. This trend might be considered as a goal of catalytic

Table 2
Catalytic properties of the potassium-doped SSWM-supported Co_3O_4 catalysts tested in this work for the ethanol steam reforming reaction.

Molar K/Co	WHSV (h^{-1})	T.O.S. (h)	T (°C)	X_{EtOH} (%)	$S^C_{CO_2}$ (%)	S^C_{CO} (%)	$S^C_{CH_4}$ (%)	S^C_C (%)	(%)	[TOF × d] $\left(g_{H_2}\ g_{Co}{}^{-1}\ s^{-1}\right)$
0.005[a]	0.72	7	411	62.6	86.2	10.5	0.4	2.9	40.2	2.8×10^{-5}
		8	386	98.3	89.2	10.6	0.2	0.0	71.9	5.1×10^{-5}
		8	360	87.4	92.1	7.9	0.0	0.0	66.5	4.8×10^{-5}
		8	411	98.6	86.0	14.0	0.0	0.0	72.9	5.2×10^{-5}
		8	386	91.5	89.0	11.0	0.0	0.0	71.6	5.1×10^{-5}
		8	360	74.2	93.0	7.0	0.0	0.0	57.6	4.1×10^{-5}
		8	334	35.4	92.8	3.9	0.0	3.3	24.7	1.7×10^{-5}
		8	309	10.4	76.4	2.6	5.7	15.3	5.8	4.1×10^{-6}
		8	283	2.8	61.0	0.7	7.6	30.6	0.6	3.9×10^{-7}
		9	411	96.7	85.2	14.8	0.0	0.0	74.0	5.3×10^{-5}
0.013[a]	0.93	7	413	98.5	84.4	15.6	0.0	0.0	81.4	7.4×10^{-5}
		8	387	98.5	85.9	14.1	0.0	0.0	85.9	7.9×10^{-5}
		8	360	98.5	87.8	12.2	0.0	0.0	89.9	8.2×10^{-5}
		8	334	72.8	92.1	7.9	0.0	0.0	65.0	5.9×10^{-5}
		8	307	19.2	79.0	4.2	5.7	10.1	10.7	9.7×10^{-6}
		8	281	3.0	67.3	4.8	15.1	12.9	1.6	1.5×10^{-6}
		8	255	0.0	–	–	–	–	0.0	0.0
		34	414	98.6	82.8	17.2	0.0	0.0	84.4	7.7×10^{-5}
0.029[b]	0.75	6	280	0.0	–	–	–	–	0.0	0.0
		8	305	0.4	46.2	7.4	46.4	0.0	0.0	0.0
		8	331	99.6	94.2	5.5	0.0	0.2	86.2	6.5×10^{-5}
		15	356	99.9	92.8	7.2	0.0	0.0	85.1	6.3×10^{-5}
		8	331	98.7	94.5	5.5	0.0	0.0	85.9	6.4×10^{-6}
		8	306	66.9	97.3	2.1	0.0	0.6	53.6	3.9×10^{-5}
		8	280	18.3	86.6	0.1	2.0	11.3	3.9	2.9×10^{-6}
		8	255	3.2	80.1	0.0	7.6	12.3	0.0	0.0
0.047[a]	0.88	10	450	99.9	66.7	8.1	0.0	25.2	78.1	6.8×10^{-5}
		10	425	99.9	67.4	7.7	0.0	24.9	76.4	6.6×10^{-5}
		10	400	100.0	66.3	7.7	0.0	26.0	74.4	6.5×10^{-5}
		10	375	94.8	63.9	6.1	0.0	30.0	67.3	5.8×10^{-5}
		10	350	46.5	51.0	3.0	0.4	45.5	26.3	2.3×10^{-5}
		10	325	15.6	38.2	2.9	7.0	51.9	6.8	5.9×10^{-6}
0.048[a]	2.73	10	450	100.0	73.4	10.7	0.0	15.8	80.2	2.2×10^{-4}
		10	425	99.8	70.5	9.2	0.0	20.3	75.9	2.0×10^{-4}
		10	400	96.5	68.2	7.2	0.0	24.6	69.0	1.9×10^{-4}
		10	370	73.9	64.6	4.2	0.0	31.2	48.3	1.3×10^{-4}
		10	345	49.8	57.0	2.5	1.6	38.8	28.4	7.7×10^{-5}
		10	320	28.8	48.2	2.3	4.7	44.8	13.9	3.8×10^{-5}
		10	295	14.1	34.3	2.2	7.3	56.2	4.8	1.3×10^{-5}
		10	275	8.0	16.1	1.1	8.1	74.8	1.4	3.7×10^{-6}
0.049[a]	2.92	20	400	74.0	72.3	10.8	0.0	16.9	56.6	1.5×10^{-4}
		10	375	50.5	68.3	8.9	2.6	20.2	36.1	9.5×10^{-5}
		10	350	30.5	72.2	7.2	6.2	14.4	22.3	5.9×10^{-5}
		10	325	14.1	59.8	14.2	11.3	14.6	8.6	2.3×10^{-5}
		10	300	6.7	30.7	35.1	14.5	19.7	2.7	7.2×10^{-6}
0.049[b]	0.79	6	283	0.0	–	–	–	–	0.0	0.0
		8	309	1.8	37.0	8.1	41.1	13.8	0.7	4.3×10^{-7}
		8	335	99.8	89.0	4.6	0.3	6.1	80.3	4.6×10^{-5}
		15	361	99.8	92.0	6.9	0.0	1.1	81.1	4.6×10^{-5}
		8	335	99.8	94.1	4.9	0.0	1.0	81.4	4.7×10^{-5}
		8	309	73.2	95.8	2.3	0.0	1.9	70.5	4.0×10^{-5}
		8	283	28.2	84.5	0.3	2.2	13.0	25.6	1.5×10^{-5}
		8	257	7.8	70.0	0.0	6.9	23.1	5.9	3.4×10^{-6}
0.058[a]	0.83	7	411	99.8	83.2	16.8	0.0	0.0	87.0	7.1×10^{-5}
		8	386	99.8	85.2	14.8	0.0	0.0	89.9	7.4×10^{-5}
		8	360	99.7	87.6	12.4	0.0	0.0	93.0	7.6×10^{-5}
		8	335	80.1	91.6	8.4	0.0	0.0	73.2	6.0×10^{-5}
		8	309	17.9	86.8	3.6	3.2	6.4	11.3	9.3×10^{-6}
		8	283	1.4	59.0	0.0	13.6	27.4	0.0	0.0
		8	258	0.0	–	–	–	–	0.0	0.0
		34	411	99.5	82.3	17.7	0.0	0.0	84.3	6.9×10^{-5}
0.085[b]	0.91	6	281	0.0	–	–	–	–	0.0	0.0
		8	307	0.4	16.1	21.0	53.9	9.0	0.2	2.0×10^{-7}
		8	334	95.4	92.6	5.5	0.0	2.0	78.3	7.1×10^{-5}
		15	360	99.8	92.6	7.4	0.0	0.0	83.1	7.4×10^{-5}
		8	334	95.2	94.6	5.4	0.0	0.0	77.3	7.0×10^{-5}
		8	307	49.3	92.0	1.4	0.0	6.5	43.9	3.9×10^{-5}
		8	281	11.5	75.5	1.5	7.7	15.3	8.8	7.8×10^{-6}
		8	255	1.5	76.5	4.0	2.7	16.9	1.3	1.2×10^{-6}
		8	229	0.0	91.4	8.6	0.0	0.0	0.2	1.4×10^{-7}

Highlighted TOF × d values used to compare the catalysts (Fig. 8). The row order is the same as the sequential order followed during the experimental tests.

[a] Calcination temperature = 400 °C.

[b] Calcination temperature = 350 °C.

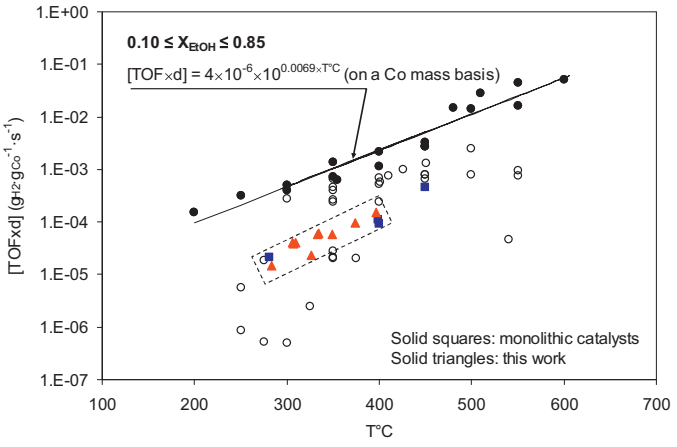

Fig. 8. Values of TOF × *d* on a Co mass basis for the catalysts prepared in this work (highlighted in Table 2) and for cobalt-based catalysts reported in the literature (Table S1 in Supplementary information).

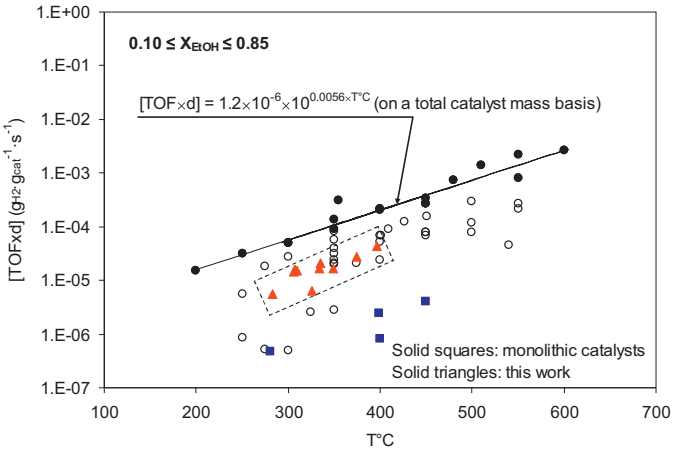

Fig. 9. Values of TOF × *d* on a total catalyst mass basis for the catalysts prepared in this work (Table 2) and for cobalt-based catalysts reported in the literature (Table S1 in Supplementary information).

activity when designing a cobalt-based catalyst for ESR. The top performing catalysts used to build the trend were:

Co(5 wt%)/Fe(0.22 wt%)/α-Al_2O_3 [33],
Na(0.2%)Co(12.5%)/ZnO [19],
Co(10%)/CeO_2/ZrO_2 [34],
Ru(0.3 wt%)Co(18 wt%)/Al_2O_3 [35],
$Ni_{0.5}Co_{0.5}O$(50 wt%)/YSZ [36],
Co(10 wt%)/CeO_2 and Co_3O_4(10 wt%)/CeO_2 [37,38] and Co(5 wt%)/$La_{0.8}Sr_{0.2}AlO_{3-\delta}$ [39]

All these catalysts display excellent turnover frequencies for the production of hydrogen, although their selectivities towards undesired carbon byproducts are high in those cases where their values are provided ($S^C_{CO_2}$ below around 70%, see Table S1). When plotting the TOF × *d* values for ethanol conversion values below 85% obtained with the potassium-doped catalysts prepared in the present work (Table 2), it can be seen that their catalytic activities are situated below the optimal trend (Fig. 8). However, comparison with the only structured catalysts (cordierite monolith-supported Co-based catalysts [9,10]) whose catalytic activity values could be calculated and plotted in Fig. 8 (solid squares) shows that the catalysts prepared in our work are similar to the catalysts supported on cordierite monoliths, on a cobalt mass basis. Moreover, if the TOF × *d* values are evaluated on a total catalyst mass basis, which also takes into account the inert support (stainless steel wire meshes in our work) then the activity of our catalysts is closer to that represented by the optimal trend (Fig. 9). Furthermore, of the structured catalysts, the SSWM-supported catalysts prepared in the present work are clearly superior to the cordierite monolith-supported catalysts on a total catalyst mass basis (Fig. 9).

4. Conclusions

In summary, the structured K-doped catalysts prepared in this work are very active and selective for the ESR reaction at low temperatures (300–350 °C), and are also very stable for long-term experiments. The active phase of these catalysts in ESR conditions is cubic CoO. The presence of potassium provokes an enlargement of the specific surface area of the catalyst and prevents its over-reduction to elemental cobalt at temperatures below 400 °C. This phase, which is predominant in undoped catalysts under low temperature ESR conditions, is highly detrimental to the ESR reaction in three ways: (i) it promotes the extensive detachment of particles from the wire mesh, (ii) it favours the deposition of coke on the surface of the particles and (iii) it provokes the undesired formation of acetone. When the active phase in ESR conditions presents $I^{200}{}_{CoO(c)}/I^{111}{}_{Co(c)}$ values higher than 1.4 (XRD spectrum) the formation of acetone does not occur.

The supported catalysts produced in this work have an activity comparable to some of the best catalysts reported in the literature and a better selectivity. Their performance is also superior to that of other structured catalysts described in literature.

Acknowledgements

The financial support for this research work provided by the Spanish MEC (CTQ2011-24776) is gratefully acknowledged. The contribution of Dr. Conchi Ovín Ania is highly appreciated.

Appendix A. Supplementary data

Supplementary material related to this article can be found, in the online version, at http://dx.doi.org/10.1016/j.apcatb.2013.12.022.

References

[1] E.Y. García, M.A. Laborde, International Journal of Hydrogen Energy 16 (1991) 307–312.
[2] Z. Khila, N. Hajjaji, M.-N. Pons, V. Renaudin, A. Houas, Fuel Processing Technology 112 (2013) 19–27.
[3] S.M. de Lima, A.M. da Silva, L.O.O. da Costa, U.M. Graham, G. Jacobs, B.H. Davis, L.V. Mattos, F.B. Noronha, Journal of Catalysis 268 (2009) 268–281.
[4] A. Haryanto, S. Fernando, N. Murali, S. Adhikari, Energy and Fuels 19 (2005) 2098–2106.
[5] M. Ni, D.Y.C. Leung, M.K.H. Leung, International Journal of Hydrogen Energy 32 (2007) 3238–3247.
[6] L.V. Mattos, G. Jacobs, B.H. Davis, F.B. Noronha, Chemical Reviews 112 (2012) 4094–4123.
[7] J.S. Moura, M.O.G. Souza, J.D.A. Bellido, E.M. Assaf, M. Opportus, P. Reyes, M.d.C. Rangel, International Journal of Hydrogen Energy 37 (2012) 3213–3224.
[8] R. Espinal, E. Taboada, E. Molins, R. Chimentao, F. Medina, J. Llorca, Topics in Catalysis (2013) 1–12.
[9] R. Espinal, E. Taboada, E. Molins, R.J. Chimentao, F. Medina, J. Llorca, Applied Catalysis B: Environmental 127 (2012) 59–67.
[10] R. Espinal, E. Taboada, E. Molins, R.J. Chimentao, F. Medina, J. Llorca, RSC Advances 2 (2012) 2946–2956.
[11] E.B. Pereira, P. Ramirez de la Piscina, S. Marti, N. Homs, Energy & Environmental Science 3 (2010) 486–492.
[12] V.c. de la Peña O'Shea, N. Homs, E.B. Pereira, R. Nafria, P. Ramírez de la Piscina, Catalysis Today 126 (2007) 148–152.
[13] B. Bayram, I.I. Soykal, D. von Deak, J.T. Miller, U.S. Ozkan, Journal of Catalysis 284 (2011) 77–89.
[14] A.M. Karim, Y. Su, M.H. Engelhard, D.L. King, Y. Wang, ACS Catalysis 1 (2011) 279–286.
[15] M. Dominguez, E. Taboada, E. Molins, J. Llorca, Catalysis Today 138 (2008) 193–197.

[16] A. Casanovas, C. de Leitenburg, A. Trovarelli, J. Llorca, Catalysis Today 138 (2008) 187–192.
[17] A. Casanovas, M. Domínguez, C. Ledesma, E. López, J. Llorca, Catalysis Today 143 (2009) 32–37.
[18] E. Lopez, A. Irigoyen, T. Trifonov, A. Rodriguez, J. Llorca, International Journal of Hydrogen Energy 35 (2010) 3472–3479.
[19] H. Lim, Journal of Membrane Science 351 (2010) 149–159.
[20] G. Marbán, I. López, T. Valdés-Solís, A.B. Fuertes, International Journal of Hydrogen Energy 33 (2008) 6687–6695.
[21] G. Marbán, A. López, I. López, T. Valdés-Solís, Applied Catalysis B: Environmental 99 (2010) 257–264.
[22] L. del Río, G. Marbán, Applied Catalysis B: Environmental 126 (2012) 39–46.
[23] T.T. Vu, L. del Río, T. Valdés-Solís, G. Marbán, Applied Catalysis B: Environmental (2013) 189–198.
[24] T.T. Vu, L. del Río, T. Valdés-Solís, G. Marbán, Journal of Hazardous Materials 246–247 (2013) 126–134.
[25] T.T. Vu, L. del Río, T. Valdés-Solís, G. Marbán, Materials Research Bulletin 47 (2012) 1577–1586.
[26] K. Asano, C. Ohnishi, S. Iwamoto, Y. Shioya, M. Inoue, Applied Catalysis B: Environmental 78 (2008) 242–249.
[27] W. Wei, W. Chen, D.G. Ivey, Chemistry of Materials 20 (2008) 1941–1947.
[28] İ. Polat, S. Aksu, M. Altunbaş, E. Bacaksız, Materials Chemistry and Physics 130 (2011) 800–805.
[29] Y. Guo, Q. Feng, Z. Dong, J. Ma, Journal of Molecular Catalysis A: Chemical 378 (2013) 273–278.
[30] W.-L. Dai, M.-H. Qiao, J.-F. Deng, Applied Surface Science 120 (1997) 119–124.
[31] I. López, T. Valdés-Solís, G. Marbán, International Journal of Hydrogen Energy 33 (2008) 197–205.
[32] I. López, T. Valdés-Solís, G. Marbán, ChemCatChem 3 (2011) 734–740.
[33] A. Kazama, Y. Sekine, K. Oyama, M. Matsukata, E. Kikuchi, Applied Catalysis A: General 383 (2010) 96–101.
[34] S.S.Y. Lin, Applied Catalysis A: General 366 (2009) 252–261.
[35] L.P.R. Profeti, E.A. Ticianelli, E.M. Assaf, Journal of Power Sources 175 (2008) 482–489.
[36] C. Resini, M. Concepción Herrera Delgado, S. Presto, L.J. Alemany, P. Riani, R. Marazza, G. Ramis, G. Busca, International Journal of Hydrogen Energy 33 (2008) 3728–3735.
[37] H. Song, B. Tan, U.S. Ozkan, Catalysis Letters 132 (2009) 422–429.
[38] H. Wang, J.L. Ye, Y. Liu, Y.D. Li, Y.N. Qin, Catalysis Today 129 (2007) 305–312.
[39] K. Urasaki, Y. Fukuda, Y. Sekine, M. Matsukata, E. Kikuchi, Journal of the Japan Petroleum Institute 51 (2008) 83–87.